Influence Of Partial Prestressing Ratio On Hysteretic Behavior Of Beam-Column Subassemblage Using Reactive Powder Concrete Materials

Siti Aisyah Nurjannah, Bambang Budiono, Iswandi Imran

Abstract: In the Indonesian and American codes of reinforced concrete design (SNI 2847:2013 and ACI 318-14, respectively) the Partial Prestressing Ratio (PPR) of a structure element is limited by 25 percent to prevent brittle behavior. Reactive Powder Concrete (RPC) materials provide high compression strength and ductility. The using of RPC allows increasing of PPR. Thus, the RPC structures provide higher nominal moment and ductility than normal concrete structures. The aim of this research was to examine the influence of PPR that exceeds 25 percent on partially pre-stressed beam-column joint sub-assemblages using RPC materials (PPRPC) to their performance. Three PPRPC specimens with PPR of 22.78 and 33.79 percent were tested according to ACI 374.1-05 loading set up. Furthermore, the finite element models of PPRPC were verified with the experiment results and also reinforced using PPR ranging from 22.78 to 41.12 percent. The results showed that the model using a PPR of 33.79 percent provided the optimum performance in terms of highest energy dissipation and ductility ranged from 11.32 to 13.46. It showed that PPRPC using RPC materials provided high performance despite the PPR level exceeds the allowed 25 percent and were suitable for structures in strong earthquake zones.

Index Terms: Beam-colum sub-assemblage, ductility, energy dissipation, finite element, partial prestressing ratio, reactive powder concrete.

1 INTRODUCTION

Reactive Powder Concrete (RPC) is concrete containing silica as the main ingredient that is reactive during the hydration process to increase the compressive strength. The material granules are micro-sized to support the compact nature of concrete [1]. To reduce the brittle behavior due to the compactness of concrete, it needs to add the microfibers made of steel or polypropylene. The use of steel fibers can increase compressive and tensile strength [2], while the use of polypropylene fibers can increase compressive strength [3], flexural, tensile and shear strength [4]. Polypropylene fibers in the RPC function as a bridge by being a link between separate pieces of concrete due to micro cracking, especially when autogenous shrinkage occurs at the beginning of the concrete's life. Microcracks are formed in the concrete drying process. The drying process generates hydration heat and results in shrinkage of the concrete volume. Polypropylene fibers can reduce bleed and increase the tensile strength of concrete [5]. In structural applications, columns using RPC materials have a better performance in holding flexural loads [6]. The aim of this study was to examine the influence of sub-assemblages using RPC materials through hysteretic behavior. Since the codes [7,8] limited the Partial Prestressing Ratios (PPR) on 25% to ensure ductility, then in this study, the PPR was varied from 22.78 to 41.12 percent and produced various energy dissipation and ductility. Concrete structures that are reinforced with partially prestressed reinforcement (a combination of steel reinforcement and prestressed strands) will be more proper to resist gravity and earthquake loads.

- *Siti Aisyah Nurjannah is a lecturer in Civil and Planning Engineering, Faculty of Engineering, Universitas Sriwijaya, Indonesia. Corresponding E-mail: sitiaisyahn@ft.unsri.ac.id*
- *Bambang Budiono and Iswandi Imran are lecturers in Structure Research Group, Civil Engineering Department, Faculty of Civil and Environmental Engineering, Institut Teknologi Bandung, Indonesia*

However, the prestressed strands must be designed to ensure the structural behavior remains ductile under earthquake loads. In a cross-section of a beam which has a partially prestressed reinforcement, if the nominal moment center is at the top concrete fiber, then the nominal moment equation is:

$$M_n = -C_s'(d') - C_c\left(\frac{d_n}{3}\right) + T_p(d_p) + T_s(d) \quad (1)$$

where M_n, C_s', C_c, T_p, T_s, d', d_n, d_p, dan d are nominal moment (unit: kN.m), steel reinforcement compressive force, concrete compressive force, prestressed strand tensile force, steel reinforcement tensile force (unit: kN), and distances from the outermost concrete fiber to the compressive steel reinforcement, concrete compressive force, prestressed strand tensile force, and tensile steel reinforcement, respectively (unit: m). In the cross-section of the beam which only has prestressed strands, the height of the concrete compressing block (a; unit: m), the concrete compressive force, and the nominal moment due to the prestressed strand (M_{np}; unit: kN.m) are expressed in equations (2, 3, and 4):

$$a = \frac{T_p}{0{,}85\, f_c' b} \quad (2)$$

$$C_c = 0{,}85\, f_c' ab \quad (3)$$

$$M_{np} = T_p d_p - C_c\left(\frac{a}{2}\right) \quad (4)$$

The hysteretic behavior of partial pre-tension precast beam-column sub-assemblage is strongly influenced by the ratio of moments contributed by the pre-tension strand to the total moment in the beam connection with the column [9,10,11]. The ratio of moments contributed by the pre-tension strand to the total moment in the beam-column joint is referred to PPR stated in equation (5). The greater the PPR value, the area of the hysteretic curve becomes smaller as shown in Figure 1.a. The smaller the value of PPR, the greater the ductility, so that the energy dissipation is greater and this is indicated by the shape of the hysteretic curve, the wider the area. The hysteretic curve that has a PPR of 75% has a flag-like curve

shape as shown in Figure 1.b. A Sub-assemblages with a PPR of 50% has a hysteretic curve similar to a parallelogram (Figure 1.c). The hysteretic curve with a PPR of 25% has the shape of the hysteretic curve as shown in Figure 1.d. Sub-assemblages that do not have a pre-strained strand (PPR = 0%) will form a hysteretic curve as in Figure 1.e under the lateral cyclic load. In ensuring the sub-assemblages remain ductile under earthquake loads to dissipate energy properly, the PPR for normal concrete is limited to 25% [7,8].

$$PPR = \frac{M_{np}}{M_n} \quad (5)$$

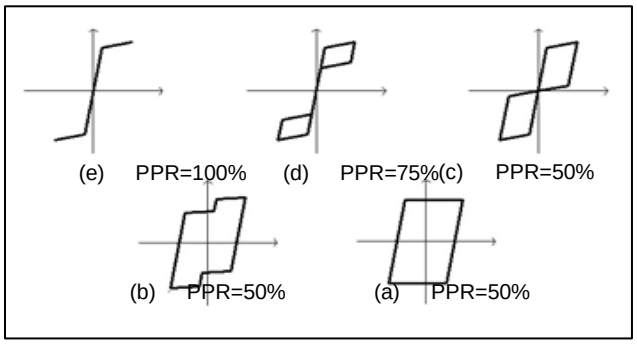

***Fig. 1**. Re-centering comparison variation effects: contribution of Dissipation to the flag-shape hysteretic curve [12].*

2 METHODOLOGY

2.1 Experimental Works

All RPC beam-column sub-assemblage reinforcement details are shown in Figure 2. There are some differences in PPR and spaces in the beam plastic hinges in Table 1. The test was conducted at the Building Structure and Construction Laboratory of Ministry of Public Works and Human Settlements. The lateral cyclic loads in the lateral column were based on displacement-control and started from a 0.20% drift ratio for three cycles and continued to be increased up to a 3.50% drift ratio on the 3rd cycle. If possible, the test is continued up to the 5.00% drift ratio on the 3rd cycle [13]. In order to observe the accuracy of the test set up, the drift ratio at the start of loading was 0.10% and 0.14% for three cycles. Every three loading cycles were interspersed with one relaxation cycle. The testing set-up of a beam-column sub-assemblage specimen is shown in Figure 3. The loading history is as shown in Table 2.

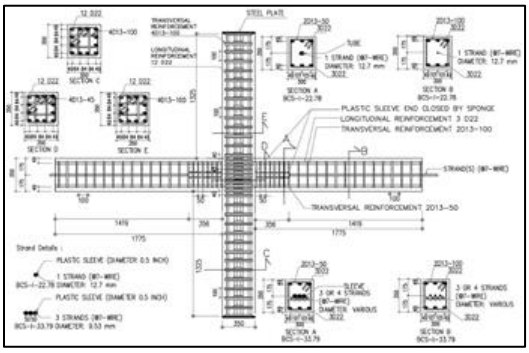

***Fig. 2.** Detail specimens of interior beam-column sub-assemblage.*

TABLE 1
PPR AND SPACES ON BEAM PLASTIC HINGES OF SPECIMENS

Strand	Specimen	PPR	Space on beam plastic hinges	M_n
		(%)	(mm)	(kN.m)
1 D12.7	S-22.78	22.78	50	135.02
3 D9.5	S-33.79	33.79	50	149.70
3 D9.5	S-33.79-A	33.79	100	149.70

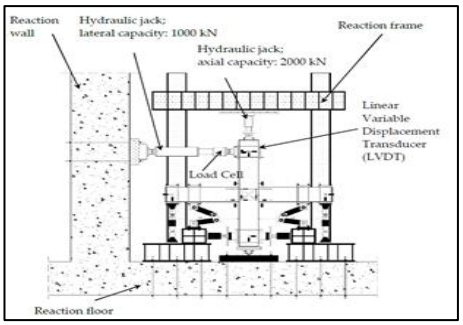

***Fig. 3**. Loading set up on an interior beam-column sub-assemblage specimen.*

TABLE 2
HISTORICAL LATERAL LOAD BASED

Loading step	Drift ratio (%)	Loading step	Drift ratio (%)
#1	0.20	#7	1.40
#2	0.25	#8	1.75
#3	0.35	#9	2.20
#4	0.50	#10	2.75
#5	0.75	#11	3.50
#6	1.00	#12	5.00

2.2 Finite Element Method

The results of specimen testing were compared with finite element modeling using ANSYS program. By using the Newton-Raphson method, iteration processes in solving nonlinear equations in the form of the equations (6) and (7) had been conducted.

$$[K_i^T]\{\Delta u_i\} = \{F^a\} - \{F_i^{nr}\} \quad (6)$$

$$\{u_{i+1}\} = \{u_i\} + \{\Delta u_i\} \quad (7)$$

where $[K_i^T]$, $\{u_i\}$, and $\{F_i^{nr}\}$ were structural stiffness matrices, degrees of freedom vectors, and working load vectors, respectively. Figure 4 shows the next iteration solution. The solution obtained at the end of the iteration process from the load factor $\{F_i^{nr}\}$ equals $\{F\}$, or approaches a certain tolerance value.

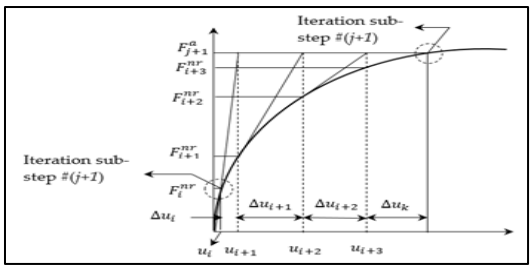

***Fig.4**. Newton-Raphson iteration in a loading sub-step*

2.3 Beam-Column Sub-assemblage Modeling

The input data of the stress-strain relationship and compressive strength of Reactive Powder Concrete are from the material test results. The dimensions and reinforcement of M-22.78, M-33.79, and M-33.79-A models were the same as S-22.78, S-33.79, and S-33.79-A specimens. To analyze the effect of Partial Prestressing Ratio (PPR) on energy dissipation, ductility and lateral forces, additional models of M-34.69, M-38.69, and M-41.12 were also analyzed. The greater the value of PPR, the nature of ductility and the ability to participate in energy will be smaller [12]. The selected strand types were 9.5 mm and 1.7 mm in diameter (D9.5 and D12.7, respectively) and used in structural experiments with nominal moment values (M_n) in Table 3. Figure 5 shows the finite element model.

TABLE 3
PPR AND NOMINAL MOMENTS OF MODELS

Strands	*Model*	*PPR*	M_n
		(%)	*(kN.m)*
1 D12.7	*M-22.78*	*22.78*	*135.02*
3 D9.5	*M-33.79*	*33.79*	*149.70*
1 D12.7 + 2 D9.5	*M-34.69*	*34.69*	*158.45*
2 D12.7 + 1 D9.5	*M-38.69*	*38.69*	*165.58*
4 D9.5	*M-41.12*	*41.12*	*161.75*

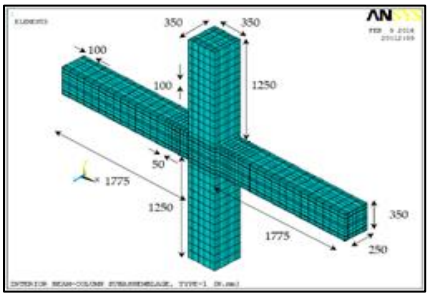

Fig.5*. A beam-column sub-assemblage model (unit: mm).*

3 RESULTS AND DISCUSSION

3.1 Modeling the Results of Material Testing

The results of compressive tests on cylindrical specimens in the form of stress-strain curves on RPC cylinders were modeled by equations (8 to 10) [14,15]. Figure 7 shows that the M1A, M2A, M3A, and M4A model-curves according to the equations resemble the M1, M2, M3, and M4 test-curves.

$$f_c = f_c' \left[\frac{\beta\left(\frac{\varepsilon}{\varepsilon_o}\right)}{\beta - 1 + \left(\frac{\varepsilon}{\varepsilon_o}\right)^{\beta}} \right] \quad (8)$$

$$\beta = \frac{1}{1 - \left(f_c'/\varepsilon_o E_{it}\right)} \quad (9)$$

$$E_{it} = 10300\,(f_c')^{0,3} \quad (10)$$

where f_c, f_c', β, ε, ε_o, and E_{it} are concrete compressive strength, characteristic concrete compressive strength (unit: MPa), material parameters that depend on the shape of the stress-strain curve, concrete strain, concrete strain when maximum compressive strength achieved, and concrete elastic modulus (unit: MPa), respectively. The concrete compressive strength used as an input model was 101.79 MPa [16].

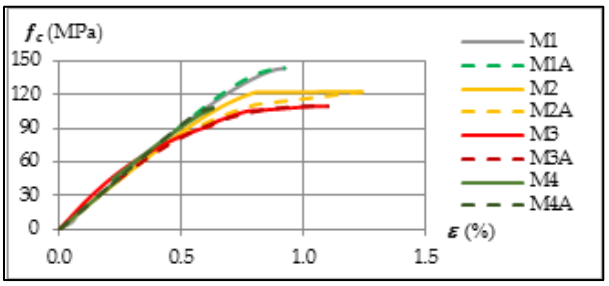

Fig. 7*. The tension-strain model-curves and test-curves.*

3.2 Verification of finite element modeling with the test results

The finite element modeling was verified with the test results by comparing the hysteretic and backbone curves in Figures 8.a to 12.d. They show the lateral forces and the displacement relation of test results and modeling. The model curves were able to approach the test result curves. The difference of lateral force (F) of the finite element modeling to the test results varied in each drift ratio (dr). In certain drift ratios, the difference was far enough due to the decreased strength of the model that was caused by the cracks on some elements, then these elements no longer contributed strength and rigidity. This did not occur in the specimen, because even though it had cracked, the part of the specimen that was still intact had strength and stiffness. The minimum story drift that should be achieved in the tests was 3.50% and if possible, the test would be continued until the story drift of 5.00% [13]. The comparison of the hysteretic curves in the story drift of 3.50% and 5.00% showed that the model-curves can approach the test-curves.

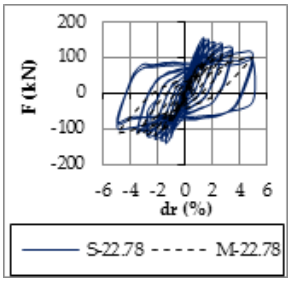

(a) Hysteretic curves up to drift ratio of 5.00%

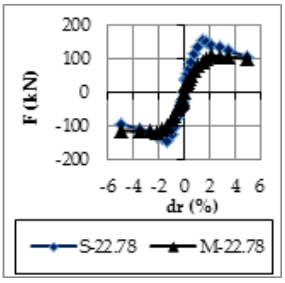

(b) Backbone curves up to drift ratio of 5.00%

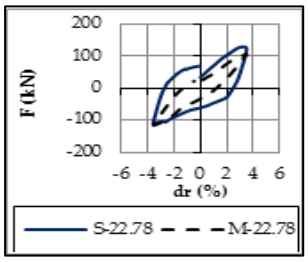

(c) Hysteretic curves at a drift ratio of 3.50%

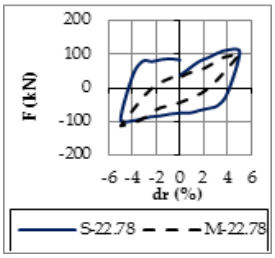

(d) Hysteretic curves at a drift ratio of 5.00%

Figure 8. *Hysteretic and backbone curves of S-22.78 specimens and M-22.78 models*

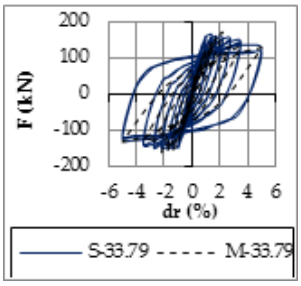

(a) Hysteretic curves up to drift ratio of 5.00%

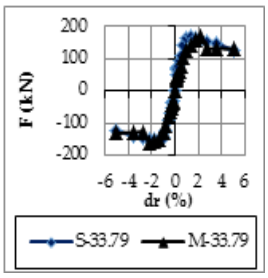

(b) Backbone curves up to drift ratio of 5.00%

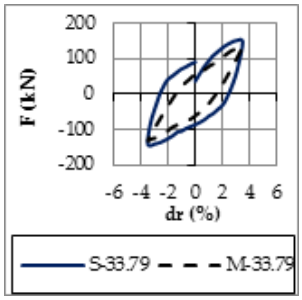

(c) Hysteretic curves at a drift ratio of 3.50%

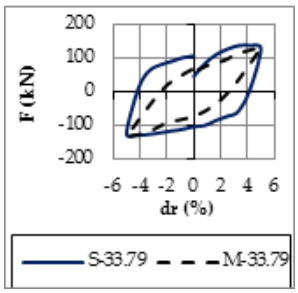

(d) Hysteretic curves at a drift ratio of 5.00%

Figure 9. *Hysteretic and backbone curves of S-33.79 specimens and M-33.79 models*

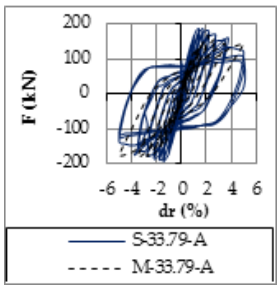

(a) Hysteretic curves up to drift ratio of 5.00%

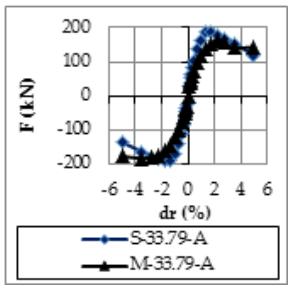

(b) Backbone curves up to drift ratio of 5.00%

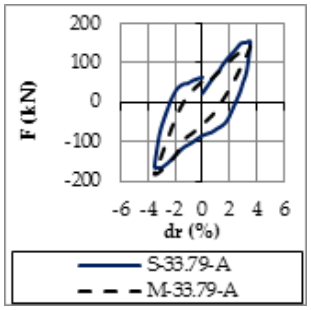

(c) Hysteretic curves at a drift ratio of 3.50%

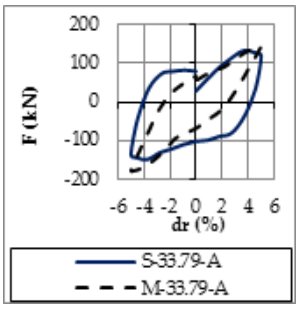

(d) Hysteretic curves at a drift ratio of 5.00%

Figure 10. *Hysteretic and backbone curves of S-33.79-A specimens and M-33.79-A models*

3.3 The Effect of Partial Prestressing Ratio on Hysteretic Curves and Lateral Force

The hysteretic curves of the five models are shown in Figure 11. The M-22.78 model curve had the smallest area and lateral force because of its smallest nominal moment. The M-33.79 model curve had the largest area because the nominal moment was sufficiently high and ductile, then it achieved a drift ratio of -5.00% (pull-load). The M-34.69, M-38.69, and M-41.12 model curves only achieved a drift ratio of + 5.00% (push-load) and did not achieve a drift ratio of -5.00% (pull-load). This was because the PPR values were too high then caused brittle behavior and the drift ratio of -5.00% (pull-load) had not achieved. The addition of PPR values from 22.78% to 34.69% resulted in an increased lateral force (F), while a PPR of 38.69% and 41.12% did not increase the lateral force significantly. The model backbone curves in Figure 12 show the maximum drift ratio and lateral force achieved by all models. The addition of PPR caused brittle behavior that caused the model with PPR of 34.69%, 38.69%, and 41.12% only achieved a drift ratio of + 5.00% (push-load) and did not achieve a drift ratio of -5.00% (pull-load). In large drift ratios under push-loads, decreased lateral forces occurred on the models with PPR of 33.79% s.d. 38.69% ($\Delta F = F_{end} - F_{peak}$) between 3.68% to 12.93% (Tables 4 and 5) after achieving the peak force with gradient difference $\{\Delta_{\text{gradient}} = (F_{peak}/\delta_{peak}) - (F_{post\ peak}/\delta_{post\ peak})\}$ ranging from 0.71 to 0.78. In a model with a PPR of 41.12%, a large nominal moment caused the model to achieve a maximum lateral force, then the lateral force decreased by 5.00% with a smaller gradient of 0.47. In high drift ratios under pull-loads, after achieving the peak force, the decreased lateral forces occurred on models with PPR of 33.79% and 38.69% as much as 2.95% and 3.95% with gradient differences of 0.43 and 0.79 (Tables 6 and 7), respectively.

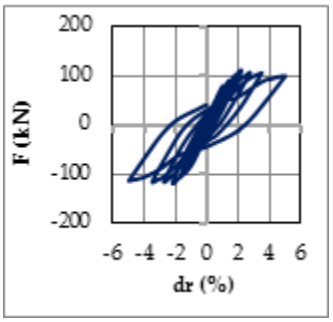

(a) M-22.78

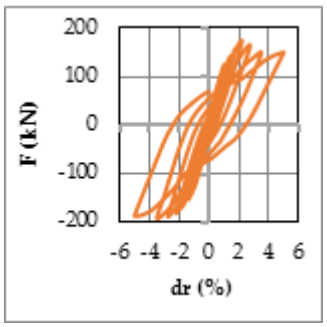

(b) M-33.79

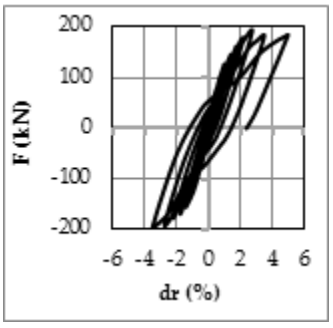

(b) M-34.69

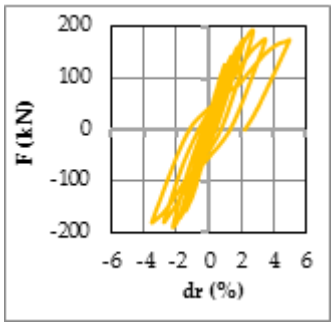

(c) M-38.69

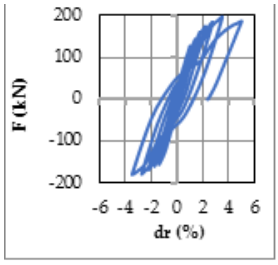

(e) M-41.12

Figure 11. *Model hysteretic curves*

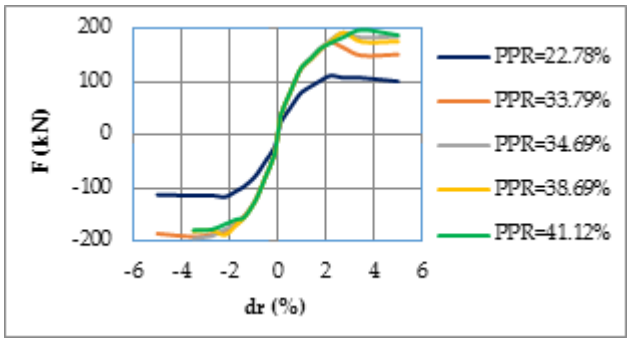

Figure 12. *Backbone model curves*

TABLE 4
THE DIFFERENCES OF LATERAL FORCE UNDER PUSH-LOADS

No.	PPR	Peak drift ratio	F_{peak}	F_{end}	δ_{peak}
	(%)	(%)			
1	22.78	2.20	110.98	100.26	64.78
2	33.79	2.20	173.28	150.87	56.77
3	34.69	2.75	192.04	184.98	70.94
4	38.69	2.75	191.93	175.25	71.34
5	41.12	3.50	197.12	187.26	91.94

TABLE 5
THE DIFFERENCES OF LATERAL FORCE UNDER PUSH-LOADS

No.	PPR	Peak drift ratio	$F_{post\ peak}$	$\delta_{post\ peak}$	ΔF	$\Delta_{gradien}$
	(%)	(%)			(%)	
1	22.78	2.20	106.88	81.20	9.66	0.40
2	33.79	2.20	163.33	71.15	12.93	0.76
3	34.69	2.75	182.62	91.53	3.68	0.71
4	38.69	2.75	174.65	91.42	8.69	0.78
5	41.12	3.50	187.26	111.81	5.00	0.47

TABLE 6
THE DIFFERENCES OF LATERAL FORCE UNDER PULL-LOADS

No.	PPR	Peak drift ratio	F_{peak}	F_{end}	δ_{peak}
	(%)	(%)			
1	22.78	2.20	116.82	112.90	64.75
2	33.79	3.50	191.60	185.94	90.79
3	34.69	3.50	195.20	195.20	90.59
4	38.69	2.20	188.54	181.09	56.95
5	41.12	3.50	179.84	179.84	91.83

TABLE 7
THE DIFFERENCES OF LATERAL FORCE UNDER PULL-LOADS

No.	PPR	Peak drift ratio	$F_{post\ peak}$	$\delta_{post\ peak}$	ΔF	$\Delta_{gradien}$
	(%)	(%)			(%)	
1	22.78	2.20	113.81	81.11	3.35	0.40
2	33.79	3.50	185.94	110.39	2.95	0.43
3	34.69	3.50	-	-	0.00	-
4	38.69	2.20	179.61	71.20	3.95	0.79
5	41.12	3.50	-	-	0.00	-

3.4 The Effect of Partial Prestressing Ratio on Energy Dissipation

The energy dissipation is spread by structures through non-linear behavior mechanisms. The amount of energy dissipation can be described as the area of the hysteretic curve. The wider the hysteretic curve, the greater the energy dissipation. The effect of PPR on energy dissipation is shown in Tables 8 and 9. Energy dissipation on specimens with PPR of 33.79% was greater than specimens with PPR of 22.78% because the higher beam nominal moments produced the ability to deform and achieve higher lateral forces. In modeling, the biggest energy dissipation was generated by a model with a PPR of 33.79%. The models with PPR of 34.69% to 41.12% were too brittle, so they only achieved a drift ratio of + 5.00% (push-load) and did not achieve a drift ratio of -5.00% (pull-load), then the ratio of energy dissipation of the models with PPR of 22.78%, 33.79%, 34.69%, 38.69%, and 41.12% were 0.68: 1.00: 0.72: 0.63: 0.73. The greater energy dissipation of the models with a PPR of 41.12% than 38.69% was due to the pre-tension strand that produced greater nominal strength, then reduced decrease lateral forces at large drift ratios. Table 10 and Figure 13 show the cumulative energy dissipation values for each specimen and model. The energy dissipation values of the models were dissimilar from the specimens' due to different lateral forces.

TABLE 8
ENERGY DISSIPATION

No.	PPR (%):	22.78	33.79
	Drift Ratio	E_d	E_d
	(%)	(kN.mm)	(kN.mm)
1	0.10	5.00	7.06

No.	PPR (%): / Drift Ratio (%)	22.78 E_d (kN.mm)	33.79 E_d (kN.mm)
2	0.14	5.28	7.21
3	0.20	10.15	14.39
4	0.25	13.14	18.04
5	0.35	27.41	25.55
6	0.50	50.27	68.18
7	0.75	87.58	123.19
8	1.00	174.28	262.23
9	1.40	792.77	1122.08
10	1.75	1278.18	1650.36
11	2.20	2754.54	3882.50
12	2.75	4972.02	7237.56
13	3.50	9119.12	13971.06
14	5.00	14554.04	21612.60
$E_{d\ cumulative}$:		33843.78	50001.99
$E_{d\ cumulative}/E_{d\ maximum\ cumulative}$:		0.68	1.00

TABLE 9
ENERGY DISSIPATION

No.	PPR (%): / Drift Ratio (%)	34.69 E_d (kN.mm)	38.69 E_d (kN.mm)	41.12 E_d (kN.mm)
1	0.10	6.77	6.75	6.77
2	0.14	6.91	6.80	7.39
3	0.20	13.83	14.27	14.16
4	0.25	18.47	18.26	18.53
5	0.35	33.25	33.11	36.74
6	0.50	70.47	71.68	70.46
7	0.75	119.85	122.60	124.90
8	1.00	263.55	263.67	262.53
9	1.40	1125.05	1137.41	1140.29
10	1.75	1671.03	1888.28	1762.51
11	2.20	3663.52	3834.03	4064.65
12	2.75	7206.37	6777.51	7622.28
13	3.50	14403.88	12351.16	13446.27
14	5.00	7369.06	4987.49	7796.06
$E_{d\ cumulative}$:		35972.00	31513.02	36373.55
$E_{d\ cumulative}/E_{d\ maximum\ cumulative}$:		0.72	0.63	0.73

TABLE 10
COMPARISON OF ENERGY DISSIPATION OF SPESIMENS AND MODELS

Spesimen atau Model	PPR	Disipasi Energi Kumulatif $E_{d\ Kumulatif}$ (%)	$E_{d\ Kumulatif}$ (kN.m)
S-22.78	22.78	22.78	252.82
M-22.78	22.78	22.78	101.53
S-33.79	33.79	33.79	317.81
S-33.79-A	33.79	33.79	263.87
M-33.79	33.79	33.79	150.01
M-34.69	34.69	34.69	107.92
M-38.69	38.69	38.69	94.54
M-41.12	41.12	41.12	109.12

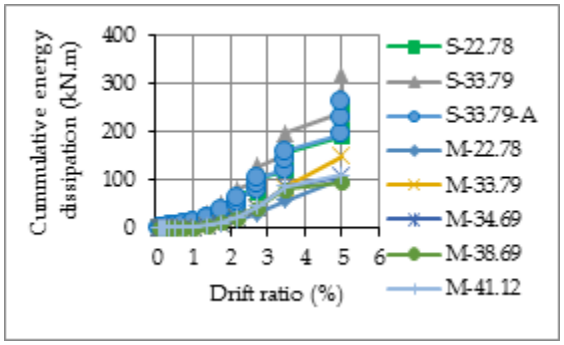

Figure 13. *Cumulative energy dissipation*

3.5 The Effect of Partial Prestressing Ratio on Ductility

The displacement ductility is defined as the ratio between the ultimate deflection to yield. The models with PPR of 22.78% and 33.79% achieved the ultimate conditions at a drift ratio of 2.75% and 5.00%, respectively. The models with PPR of 34.69%, 38.69%, and 41.12% achieved the ultimate conditions at a drift ratio of 3.50%. This was due to the pre-stressed strand of the model with a PPR of 33.79% provided higher nominal strength at a large drift ratio and was properly ductile, while the models with a PPR of 34.69% to 41.12% were more brittle. The yield points due to push (+) and pull (-) loads were determined by the area method [17]. The stiffness and lateral ultimate deflection of models are shown in Tables 11 to 14. The stiffness and lateral ultimate deflection of specimens are shown in Tables 15 to 18. The ultimate condition of the model was defined as 75% lateral peak force [13]. The comparison of the ductility of each specimen and model is shown in Table 19. The ductility values of the model were close to the specimens'.

TABLE 11
THE STIFFNESS OF SPECIMENS

Specimens	Yield deflection		Yield lateral force	
	δ_y (+) (mm)	δ_y (-) (mm)	F_y (+) (kN)	F_y (-) (kN)
	(1)	(2)	(3)	(4)
S-22.78	8.35	8.05	89.30	55.90
S-33.79	8.10	8.05	112.20	91.00
S-33.79-A	7.00	7.20	103.20	109.20

TABLE 12
THE STIFFNESS OF SPECIMENS

Specimens	Stiffness	
	K_y (+)	K_y (-)
	(kN/mm)	(kN/mm)
	(5) = (3)/(1)	(6) = (4)/(2)
S-22.78	10.69	6.94
S-33.79	13.85	11.30
S-33.79-A	14.74	15.17

TABLE 13
THE LATERAL ULTIMATE DEFLECTION OF SPECIMENS

Model	Ultimate drift ratio (+)	Lateral ultimate deflection (+)
		□
	(%)	(mm)
S-22.78	3.50	88.02
S-33.79	3.50	83.64
S-33.79-A	3.50	76.17

TABLE 14
THE LATERAL ULTIMATE DEFLECTION OF SPECIMENS

Model	Ultimate drift ratio (-)	Lateral ultimate deflection (-)
		□
	(%)	(mm)
S-22.78	3.50	87.90
S-33.79	3.50	83.73
S-33.79-A	3.50	76.11

TABLE 15
THE STIFFNESS OF MODELS

Model	Yield deflection		Yield lateral force	
	δ_y (+)	δ_y (-)	F_y (+)	F_y (-)
	(mm)	(mm)	(kN)	(kN)
	(1)	(2)	(3)	(4)
M-22.78	9.80	-8.20	48.90	-48.99
M-33.79	9.80	-8.20	77.58	-128.54
M-34.69	9.80	-8.20	77.55	-129.71
M-38.69	9.80	-8.20	104.63	-78.51
M-41.12	9.80	-8.20	78.17	-129.76

TABLE 16
THE STIFFNESS OF MODELS

Model	Stiffness	
	K_y (+)	K_y (-)
	(kN/mm)	(kN/mm)
	(5) = (3)/(1)	(6) = (4)/(2)
M-22.78	4.99	5.97
M-33.79	7.92	15.68
M-34.69	7.91	15.82
M-38.69	10.67	9.57
M-41.12	7.97	15.82

TABLE 17
THE LATERAL ULTIMATE DEFLECTION OF MODELS

Model	Ultimate drift ratio (+)	Lateral deflection (+)
		δ
	(%)	(mm)
M-22.78	2.75	81.20
M-33.79	5.00	110.95
M-34.69	3.50	91.53
M-38.69	3.50	91.42
M-41.12	3.50	91.94

TABLE 18
THE LATERAL ULTIMATE DEFLECTION OF MODELS

Model	Ultimate drift ratio (-)	Lateral deflection (-)
		δ
	(%)	(mm)
M-22.78	2.75	81.11
M-33.79	5.00	110.39
M-34.69	3.50	90.59
M-38.69	3.50	90.70
M-41.12	3.50	91.83

TABLE 19
COMPARISON OF SPECIMEN AND MODEL DUCTILITIES

Specimen and Model	PPR	Ductility (+)	Ductility (-)
		μ	μ
	(%)		
S-22.78	22.78	8.25	8.63
M-22.78	22.78	8.28	9.89
S-33.79-A	33.79	8.55	10.57
S-33.79	33.79	10.33	10.40

Specimen and Model	PPR	Ductility (+)	Ductility (-)
		μ	μ
	(%)		
M-33.79	33.79	11.32	13.46
M-34.69	34.69	9.34	11.05
M-38.69	38.69	9.33	11.06
M-41.12	41.12	9.38	11.20

3.6 The Effect of Partial Prestressing Ratio on the Degradation of Strength and Rigidity

The strength degradation is the ratio between a lateral force (F) and the lateral yield force (F_y). The stiffness degradation is the ratio between a stiffness (K) and the yield (K_y). The strength degradation (F/F_y) and stiffness degradation (K/K_y) of each model are shown in Figures 14 and 15. The PPR contributed to the nominal moment of the beams. The smaller the PPR, the greater the strength and stiffness degradation.

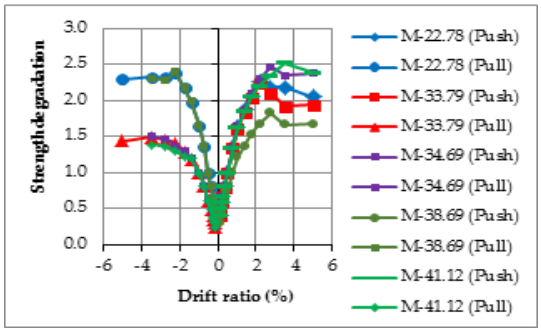

Figure 14. *Degradation of strength*

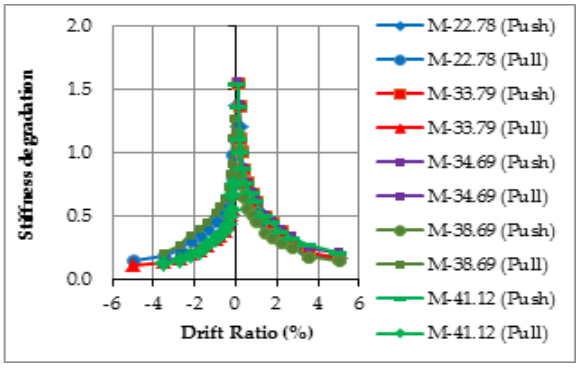

Figure 15. *Degradation of stiffness*

3.6 The Effect of Partial Prestressing Ratio on Ultimate Lateral Force

The differences in lateral forces of each model in the ultimate conditions under push and pull-loads are shown in Tables 20 and 21, respectively. The PPR affected the lateral forces. The largest maximum lateral forces under push and pull-loads were achieved by the M-41.12 and M-34.69 models. This difference was because the M-41.12 model with the largest PPR provided the greatest strength under push-loads at a large drift ratio. The brittle behavior of the model with large PPR caused decreased forces under pull-load conditions at the same drift ratio.

TABLE 20
LATERAL FORCE COMPARISON UNDER PUSH-LOADS

Models	Ultimate drift ratio (+)	Maximum lateral force (+)	Comparison of lateral force (+)
		F	$F/F_{maximum}$
	(%)	(kN)	
M-22.78	2.75	106.88	0.54
M-33.79	5.00	150.87	0.77
M-34.69	3.50	182.62	0.93
M-38.69	3.50	174.65	0.89
M-41.12	3.50	197.12	1.00

TABLE 21
LATERAL FORCE COMPARISON UNDER PULL-LOADS

Model	Ultimate drift ratio (-)	Maximum lateral force (-)	Comparison of lateral force (-)
		F	$F/F_{maximum}$
	(%)	(kN)	
M-22.78	2.75	-113.81	0.58
M-33.79	5.00	-185.94	0.95
M-34.69	3.50	-195.20	1.00
M-38.69	3.50	-181.09	0.93
M-41.12	3.50	-179.84	0.92

4 CONCLUSION

From the study, there are some derived conclusions:

1. The modeling of beam-column sub-assemblages had been verified using hysteretic curves of experimental results of specimens with a Partial Prestressing Ratio (PPR) of 22.78% and 33.79%.
2. The models were developed further by increasing the PPR to 34.69%, 38.69%, and 41.12%. The PPR influenced the performance of models in terms of nominal moment, ductility, and energy dissipation.
3. By reviewing the lateral forces, cumulative energy dissipation, and displacement ductility, the M-33.79 model with a PPR of 33.79% provided the optimum performance.
4. The M-22.78 model with PPR of 22.78% had a strength degradation and stiffness degradation faster than other models with higher PPR. All models with higher PPR than 33.79% had less ductility and energy dissipation than the model with PPR of 33.79% due to the brittle behavior.

5 RECOMMENDATIONS

There are two recommendations for further study:

1. A proposed installation of partially pre-stressed reinforcement using PPR of 33.79% to increase the strength of structural elements to resist seismic loads. In this case, the material of concrete is Reactive Powder Concrete with a sufficient volume fraction of polypropylene fibers to provide ductility and energy dissipation.
2. The use of micro steel fibers to replace polypropylene fibers for improving the ductility of RPC, thus increasing the

level of Partial Prestressing Ratio, energy dissipation, and the beam nominal moments.

6 ACKNOWLEDGMENT

All authors wish to thank to P.T. Wijaya Karya Beton, Indonesia for supporting this research.

7 REFERENCES

[1] M. Lanez, M.N. Oudjit., and A. Bali, “Reactivity of Cementitious Additions on Properties of Micro”, Procedia - Social and Behavioral Sciences 195, pp. 2336 – 2342, 2015.

[2] Y. Zhang, B. Wu, J. Wang, M. Liu, and X. Zhang, “Reactive Powder Concrete Mix Ratio and Steel Fiber Content Optimization under Different Curing Conditions”, Journal of Materials, 12, 3615, pp. 1-19, 2019, doi:10.3390/ma12213615.

[3] C.C. Patil, dan P. Shivananda, “Experimental Study on the Performance of Polypropylene Fiber Reinforced Concrete”, International Journal of Application or Innovation in Engineering & Management, Volume 6, Issue 8, pp. 114-119, 2017.

[4] K. Murahari and R. Rao, “Effects of polypropylene fibers on the strength properties of fly ash based concrete”, International Journal of Engineering Science Invention, 2(5), p. 13-19, 2013.

[5] J. Newman dan B.S. Choo, Advanced Concrete Technology Part 1 and 2: Constituent Materials. Elsevier, Oxford, 2003.

[6] M.N.S. Hadi, A.H.M. Algburi, M.N. Sheikh, A.T. Carrigan, “Axial and flexural behavior of circular reinforced concrete columns strengthened with reactive powder concrete jacket and fiber-reinforced polymer wrapping”, Construction and Building Materials, Vol. 172, pp. 717–727, 30 May 2018.

[7] Badan Standardisasi Nasional (BSN), SNI 03-2847-2013 Tata Cara Perhitungan Struktur Beton untuk Bangunan Gedung, BSN, Jakarta, Indonesia, especially article 21.5.2.5 (b, c), 2013.

[8] ACI Committee 318, Building Code Requirements for Structural Concrete (ACI 318-14) and Commentary, American Concrete Institute, Farmington Hills, USA, especially article 18.6.3.5 (b, c), 2014.

[9] J.F. Stanton, W.C. Stone, dan G.S. Cheok, “A Hybrid Reinforced Precast Frame for Seismic Regions”, Precast/Prestressed Concrete Institute Journal, Vol. 42, No. 2, pp. 20-32, 1997.

[10] M.J.N. Priestley, “Direct Displacement-Based Design of Precast/Prestressed Concrete Buildings”, Precast/Prestressed Concrete Institute Journal, Vol. 47, No.6, pp. 66-78, 2002.

[11] ACI Innovation Task Group 1 and Collaborators, Special Hybrid Moment Frames Composed of Discretely Jointed Precast and Post-Tensioned Concrete Members (ACI T1.2-03.) and Commentary (ACI T1.2R-03), American Concrete Institute, Farmington Hills, USA, 2003.

[12] S. Pampanin, D. Marriott, A. Palermo, and D. Bolognini, PRESSS Design Handbook, New Zealand Concrete Society, Auckland, 2010.

[13] ACI Committee 374, Acceptance Criteria for Moment Frames Based on Structural Testing and Commentary (ACI 374.1-05), Farmington Hills, USA, 2005.

[14] D.J. Carreira and K.H. Chu, “Stress-strain Relationship for Plain Concrete in Compression”, ACI Material Journal, No. 83 (6), pp. 797-804, 1985.

[15] T.H. Wee, M.S. Chin, and M.A. Mansur, “Stress-strain Relationship of High Strength Concrete in Compression”, ASCE Journal of Materials in Civil Engineering, Vol. 8, No. 2, pp. 70-76, May 1996.

[16] S.A. Nurjannah, B. Budiono, I. Imran, and S. Sugiri, “The Hysteretic Behavior of Partially Pre-Stressed Beam-Column Joint Sub-Assemblages Made of Reactive Powder Concrete”, Journal of Engineering and Technological Sciences, 48(5), pp. 550-570, 2016.

[17] American Society of Civil Engineers (ASCE), Federal Emergency Management Agency (FEMA) 356 Prestandard and Commentary for the Seismic Rehabilitation of Buildings, Virginia, pp. 3-19 to 3-20, 2000.